

The role of the interface in controlling the epitaxial relationship between orthorhombic LaInO_3 and cubic BaSnO_3

Martina Zupancic¹, Wahib Aggoune², Toni Markurt¹, Youjung Kim³,
Young Mo Kim³, Kookrin Char³, Claudia Draxl², and Martin Albrecht¹

¹*Leibniz-Institut für Kristallzüchtung, Max-Born-Str. 2, 12489 Berlin, Germany*

²*Institut für Physik and IRIS Adlershof, Humboldt-Universität zu Berlin, 12489 Berlin, Germany*

³*Institute of Applied Physics, Dept. of Physics and Astronomy, Seoul National University, Seoul 08826, Korea*

Epitaxial perovskite oxide interfaces with different symmetry of the epitaxial layers have attracted considerable attention due to the emergence of novel behaviors and phenomena. In this paper, we show by aberration corrected transmission electron microscopy that orthorhombic LaInO_3 films grow in form of three different types of domains on the cubic BaSnO_3 pseudosubstrate. Quantitative evaluation of our TEM data shows that c_{pc} -oriented and a_{pc}/b_{pc} -oriented domains are present with similar probability. While continuum elasticity theory suggests that c_{pc} -oriented domains should exhibit a significantly higher strain energy density than a_{pc}/b_{pc} -oriented domains, density functional calculations confirm that c_{pc} - and a_{pc} -oriented domains on BaSnO_3 have similar energies.

I. INTRODUCTION

Over the last decade, many studies have focused on polar - non-polar perovskite oxide interfaces due to the promise to realize novel electronic devices, and to tune the electronic behavior between metallic, semiconducting, and superconducting [1–3]. The formation of a 2-dimensional electron gas at the interface, as well as the mobility of carriers and other physical properties, crucially depend on the atomic structure of the interface. Since most of these heterostructures are heteromorphous and consist of materials with different space groups, the crystallographic orientation relationship between them is an important issue. A common approach to predict the preferred orientation in coherently strained films is to consider the orientation that results in the lowest total energy, E_{total} , where:

$$E_{total} = E_{interface} + E_{strain}. \quad (1)$$

In classical group IV semiconductors or III-V compounds, the interface energy in most cases is negligible, and the total energy is dominated by the strain energy. The strain induced by the substrate in these systems is accommodated by a tetragonal distortion of the unit cell and can be calculated by continuum elasticity theory. Epitaxial growth of ABO_3 perovskite oxides on each other is governed by a number of peculiarities:

- Perovskites in most cases exhibit different crystal symmetry (e.g. perfect cubic, rhombohedral, orthorhombic) mediated by symmetry reducing distortions of the perfect cubic structure, often reflected in a respective tilt of the BO_6 octahedra. If, for example, a layer with lower symmetry grows coherently on a substrate with perfect cubic symmetry, different epitaxial relationships are possible.
- Perovskites can adopt strain by both, octahedral rotations (along the surface normal or perpendicular to it) and by relative displacement of

cations and anions, i.e. by distortions of the unit cell. Peculiarities of the strain accommodation will strongly depend on the chemistry of the compound [4].

- The interface may play a role in the energetics of the system. The octahedra tilt pattern of the substrate may influence the one of the epitaxial layers and counteract strain accommodation. Chemistry may then control the energy balance over strain. Another important contribution that controls interface formation is the charge that is present at a polar - non-polar interface.

In this paper, we combine quantitative high-resolution transmission electron microscopy (HRTEM) and ab-initio density functional theory (DFT) calculations to study the formation of the polar - non-polar interface between the orthorhombic perovskite LaInO_3 and the cubic perovskite BaSnO_3 . This system has attracted considerable attention in the last decade, since it enables the formation of a 2-dimensional electron gas at its interface, similar to the prototypic system LaAlO_3 on SrTiO_3 [1, 5–7]. In addition, BaSnO_3 possesses the highest electron mobility ($\sim 300 \text{ cm}^2/\text{Vs}$) among the transparent conductive oxides [8, 9].

Here we show that orthorhombic LaInO_3 grows coherently in domains with three possible orientations on the cubic BaSnO_3 pseudosubstrate. Despite significant difference in strain energy, all domains are present with similar probabilities. Since the perovskite oxides often exhibit phase transformations in the range between room temperature and typical film growth temperatures, it is not clear whether the domains form already during growth or just at a later stage of cool-down after growth. The presence of strain may also shift the transition temperatures, therefore in this work we perform TEM in-situ heating experiment to check if LaInO_3 undergoes phase transitions [10–12].

While similar observations of differently oriented domains have been made for the growth of orthorhombic

SrRuO₃ and CaRuO₃ films on cubic substrates [13, 14], a consisted explanation is not given. We show that the tilt pattern of the growing layer is controlled by the cubic substrate and causes the shifts of the total energy such that different orientations are energetically degenerated.

II. METHODS

BaSnO₃/LaInO₃ heterostructures studied in this paper were grown by Pulsed Laser Deposition (PLD) on TiO₂-terminated SrTiO₃ (001) substrates at 750 °C in 100 mTorr of oxygen pressure using KrF excimer laser with energy fluence in the range of 1.2 ~ 1.5 J/cm². All targets were provided by Toshiba Manufacturing Co. in Japan.

High-resolution TEM was performed with an aberration corrected FEI Titan 80-300 operated at 300 kV, with the corrector for spherical aberrations (Cs) set to a Cs = -15 μm. Cross-sectional TEM samples were prepared along the ⟨100⟩ lattice direction of the BaSnO₃ pseudo-substrate by tripod polishing and argon ion-milling at liquid nitrogen temperature. Ar⁺ ion-milling was done by a precision ion polishing system (PIPS) at beam energies from 4.0 to 0.2 keV. Plane-view samples were prepared by wedge polishing with a wedge angle of 4°, using the Allied MultiPrepTM system.

The lamella used for the in-situ heating TEM experiment was prepared by cutting a piece of the wedge-polished sample by focused ion beam (FIB) and transferring it by in-situ lift-out method on a Protochips' Fusion E-chip. In-situ heating experiment was conducted with a Protochips' Fusion holder. The sample was heated in vacuum with a 5 °C/s ramp rate in the temperature range from 25750 °C.

Ground-state properties are calculated using DFT, within the generalized gradient approximation (GGA) for the exchange-correlation functional in the PBEsol parameterization [15]. All calculations are performed using FHI-aims [16], an all-electron full-potential package. The code is based on numerical atom-centered orbitals. For all atomic species we use *tight* settings with the *tier 2* basis set for oxygen (O), *tier1 + fg* for barium (Ba), *tier1 + gpdf* for tin (Sn), *tier1 + hfdg* for lanthanum (La), and *tier1 + gpfhf* for indium (In). The self-consistent field convergence criteria are 10⁻⁶ electrons for the density, 10⁻⁶ eV for the total energy, 10⁻⁴/Å for the forces, and 10⁻⁴ eV for the eigenvalues. For bulk BaSnO₃ and LaInO₃, both, lattice constants and internal coordinates are optimized until the residual forces on each atom are less than 0.001 eV/Å. The sampling of the Brillouin zone is performed with an 8 × 8 × 8 k-grid for bulk BaSnO₃, and with an 6 × 6 × 4 k-grid for bulk LaInO₃. These parameters ensure a numerical precision better than 5 meV/atom for the total energy and 0.001 Å for the lattice parameters. For the BaSnO₃/LaInO₃ heterostructure, the Brillouin zone sampling is performed with an 6 × 6 × 1 k-grid for the case where the *c*_{pc} orientation

of LaInO₃ is parallel to the BaSnO₃ (001) surface, and an 4 × 4 × 1 k-grid when the *a*_{pc} orientation of LaInO₃ is parallel to the BaSnO₃ (001) surface. We include a vacuum of ~ 70 Å and apply a dipole correction in the non-periodic [001] direction, in order to prevent unphysical interactions between neighboring replica. In this case, only internal coordinates are optimized until the residual forces on each atom are less than 0.001 eV/Å. The lattice parameter of the first unit cell of the BaSnO₃ pseudo-substrate is fixed to the bulk value. To calculate the strain energy density at the BaSnO₃/LaInO₃ interfaces, we compute the elastic constants of bulk BaSnO₃ and LaInO₃ from the second derivatives of the total energy [17]. The *ElaStic* package is used to compute the second derivatives and extract the elastic constants [17]. Atomic structures are visualized using the VESTA software [18].

III. CRYSTALLOGRAPHIC CONSIDERATIONS AND BASIC MATERIALS PARAMETERS

BaSnO₃ is a perfect cubic perovskite with a lattice constant of 4.116 Å (Fig. 1 (b)) [19]. LaInO₃ has an orthorhombic structure of type GdFeO₃ (Fig. 1 (a)) with lattice parameters *a*_{ortho} = 5.9404 Å, *b*_{ortho} = 5.7229 Å, and *c*_{ortho} = 8.2158 Å, [20]. The structure of LaInO₃ is characterized by rotation of the InO₆ octahedra along all three pseudocubic directions and defined by the *a*⁻*a*⁺*c*⁺ tilt pattern according to the Glazer notation [21], which

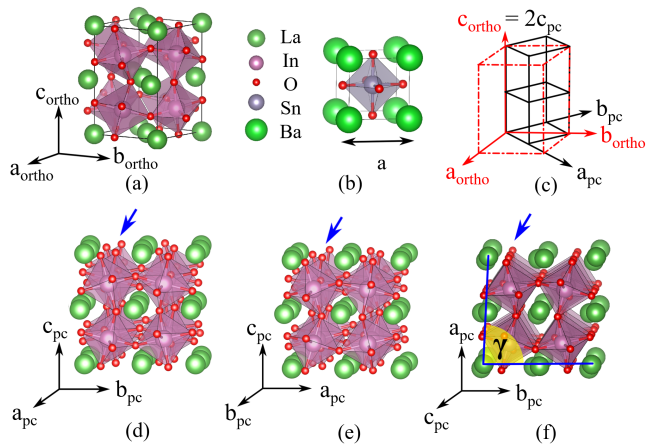


FIG. 1. Sketch of the primitive unit cell of (a) orthorhombic LaInO₃ and (b) cubic BaSnO₃. (c) Scheme of the relationship between the orthorhombic (red) and pseudocubic (black) LaInO₃ unit cell. The *a*⁻*a*⁺*c*⁺ Glazer tilt pattern describes InO₆ octahedral tilt (marked with blue arrows) in orthorhombic LaInO₃ perovskite structure: (d) *a*⁻ out-of-phase tilt around the *a*_{pc} = [100]_{pc} axis (out-of-phase tilt signifies oxygen octahedra which rotate along the pseudocubic rotational axis in opposite direction), (e) *a*⁻ out-of-phase tilt around the *b*_{pc} = [010]_{pc} axis and (f) *c*⁺ in-phase tilt around the *c*_{pc} = [001]_{pc} axis (in-phase tilt signifies oxygen octahedra which rotate along the rotational axis in the same direction). The angle between *a*_{pc} and *b*_{pc}, γ , equals 87.6°.

is described in Figs. 1 (d), (e), and (f). A scheme of the LaInO_3 orthorhombic unit cell and its correlation with the pseudocubic one is shown in Fig. 1 (c), where a_{pc} , b_{pc} , and c_{pc} represent $[100]$, $[010]$, and $[001]$ pseudocubic directions, respectively. When comparing the a_{pc} and b_{pc} film growth orientations, there is no difference with respect to the strain between them. These two orientations are the same if we compare an area larger than one unit cell. However, if we consider just one unit cell (Figs. 1 (d) and (e)), a different rotation direction around the in-plane axis for the equivalent oxygen atoms in the oxygen octahedra can be observed.

TABLE I. Experimental lattice parameters (in Å) of BaSnO_3 and LaInO_3 compared to theoretical values obtained by PBEsol (this work).

		a	b	c
BaSnO_3	Expt.	4.117 [22, 23]	-	-
		4.116 [19]	-	-
	This work	4.119	-	-
LaInO_3	Expt. [20]	5.940	5.723	8.216
	This work	5.939	5.698	8.210

Table I compares experimental lattice parameters to those calculated in this work. The computed lattice parameters of both BaSnO_3 and LaInO_3 are in good agreement with previously reported experimental values [19, 20, 22, 23], and are used in the following calculations of the strain energy density based on elastic continuum theory. In Table II, we summarize the calculated elastic constants of orthorhombic LaInO_3 which are used in the following calculations. Our results are in good agreement with previous theoretical findings based on DFT calculations reported in [24, 25]. Small differences in the elastic constants of LaInO_3 are mainly due to the differences in the lattice parameters.

IV. EXPERIMENTAL RESULTS

A. Domain distribution

$\text{BaSnO}_3/\text{LaInO}_3$ heterostructures were grown on the SrTiO_3 (001) substrate. Due to the high lattice mismatch of -5.5 %, the BaSnO_3 film grows relaxed on the SrTiO_3 substrate. Therefore, we consider BaSnO_3 as a pseudo-substrate with the bulk value of lattice parameter. Fig. 2 (a) shows typical results of a high-resolution TEM cross-section analysis of the $\text{BaSnO}_3/\text{LaInO}_3$ interface. The BaSnO_3 film/pseudosubstrate is seen along the $[010]$ projection. It is single crystalline and grows epitaxially along the $[001]$ surface normal of the SrTiO_3 substrate. The LaInO_3 film on top of the BaSnO_3 pseudosubstrate surface is characterized by three types of coherently grown 5 - 40 nm wide domains which can be distinguished by the respective image patterns (Fig. 2 (a)). In the first domain from the left (I), the c_{pc} orientation lays along the

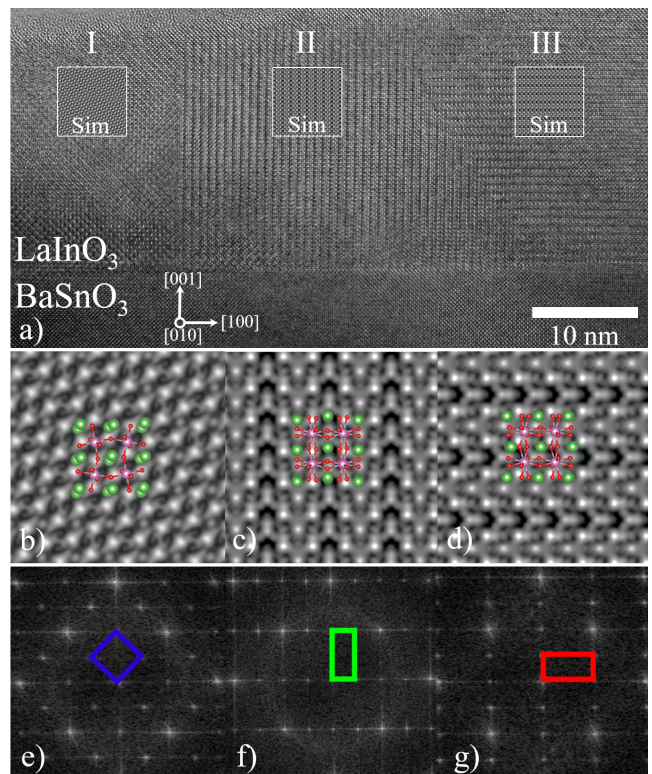


FIG. 2. (a) Cross-sectional HRTEM image of the LaInO_3 film grown on BaSnO_3 . HRTEM simulations are shown as insets. Corresponding magnified simulations are shown together with assigned atomic models in (b), (c), and (d). Fast Fourier transformed images of LaInO_3 domains are shown on (e), (f), and (g) where blue, green, and red marked unit cells correspond to the domains I, II, and III shown in (a), respectively.

$[010]$ projection of the BaSnO_3 substrate, and can be observed along the viewing direction. The image simulation highlighted by the white frame is shown as an inset and reproduces the experimental pattern of the upper part of the domain. The center and the right domain (II and III) show a stripe-like pattern with a characteristic periodicity where each fourth plane appears at lower intensity. For the chosen imaging conditions (defocus $\Delta f = +8$ nm, thickness $t = 22.9$ nm), the symmetry of the pattern reflects the symmetry of the projected unit cell. The observed periodicity corresponds to the size of the unit cell along a_{pc}/b_{pc} , and the image simulations reproduce the experimental patterns well. In the domain III, c_{pc} planes are parallel to the $[001]$ surface normal of BaSnO_3 , while in the domain II, c_{pc} planes lay parallel to (100) planes of BaSnO_3 . Since the a_{pc} and b_{pc} orientations exhibit the same atomic pattern, they cannot be distinguished from the HRTEM image pattern. They will therefore be referred to as a_{pc}/b_{pc} in the further text. Magnified simulated patterns, overlaid by ball and stick models of the atomic structure, are shown in Figs. 2 (b), (c), and (d). Fast Fourier transformed images of c_{pc} , a_{pc}/b_{pc} which is rotated by 90° clockwise/counterclockwise, and a_{pc}/b_{pc}

TABLE II. Calculated elastic constants of LaInO_3 and BaSnO_3 in GPa.

		C_{11}	C_{12}	C_{22}	C_{13}	C_{23}	C_{33}	C_{44}	C_{55}	C_{66}
BaSnO_3	Ref. [24]	285.2	68.5					84.3		
	This work	286.5	83.4					93.6		
LaInO_3	Ref. [25]	238.1	121.7	225.8	111.5	104.4	195.3	52.6	70.4	52.6
	This work	243.9	129.1	234.8	118.8	112.2	204.7	54.7	73.6	58.1

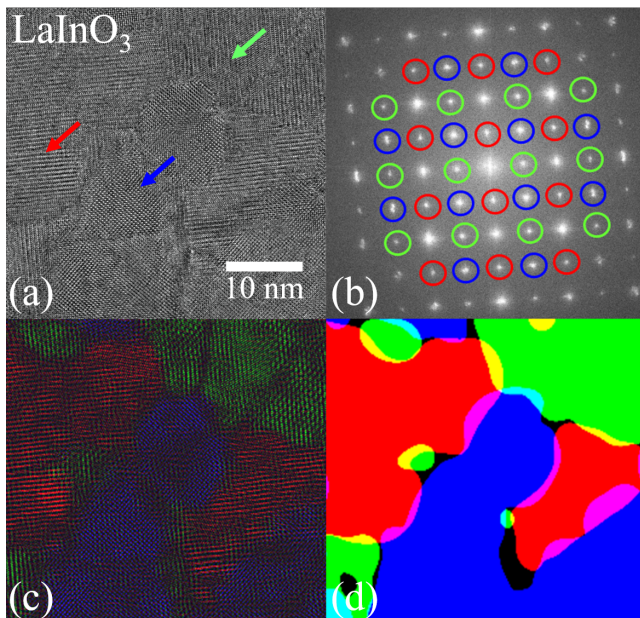


FIG. 3. (a) HRTEM image of plane-view. (b) Fast Fourier transformation of HRTEM image where red, green, and blue correspond to reflexes specific only for a_{pc}/b_{pc} orientation, a_{pc}/b_{pc} orientation that is 90° rotated in the in-plane direction compared to the previous one, and c_{pc} orientation, respectively. (c) RGB composite image of Bragg filtered areas for three different type of domains. (d) RGB composite threshold image of three different type of domains.

are shown in Figs. 2 (e), (f), and (g), respectively.

To get statistically significant results on the distribution of the different domains, we study the samples in plane-view TEM. Fig. 3 (a) shows a typical image under multibeam conditions along the $[001]$ surface normal of BaSnO_3 . Similar as in the cross-section, we assign the domains according to the orientation of the stripe-like patterns in the HRTEM images, which can be assigned to the a_{pc}/b_{pc} planes in orthorhombic LaInO_3 . To ease the analysis, we perform Bragg filtering. We select reflections in the fast Fourier transformed image that are specific for each of the three different type of domains (Fig. 3 (b)), and separately apply a mask on each set of specific reflexes. We then perform an inverse Fourier transformation for the specific reflection. By doing so, each of the filtered images shows only domains of the same chosen orientation. A composite Bragg filtered RGB image shown in Fig. 3 (c) exhibits all three type of domains. Converting filtered images further to binary

images, the occupancy percentage of each domain type can be calculated. Processed binary images are additionally combined together into the RGB image where red, green, and blue colors represent different domain orientations, a_{pc}/b_{pc} , a_{pc}/b_{pc} which is rotated by 90° in the in-plane direction, and c_{pc} orientation, respectively (Fig. 3 (d)). For quantification of the domain distribution, a total sample area of $0.4 \mu\text{m}^2$ containing approximately 1000 domains is investigated. The investigation reveals that LaInO_3 domains with c_{pc} orientation (blue) parallel to the BaSnO_3 (001) surface are occupying 44.4 % of the LaInO_3 film, while a_{pc}/b_{pc} -oriented domains (red and green) cover together 55.6 %.

B. Interface

To get an insight into the interface structure, we study a LaInO_3 domain with the a_{pc}/b_{pc} surface normal along the c_{pc} viewing direction. We focus here on the octahedral tilt, and perform exit wave reconstruction from the defocus series. Fig. 4 (a) shows the amplitude of the exit wave reconstructed from a focal series, while Fig. 4 (b) shows the inverse image, which is used for analysis by peak finding. The atomic structure of BaSnO_3 and LaInO_3 is shown as an overlay to the images. Based on the bulk properties, we expect γ angles of 90° for BaSnO_3 and of 87.6° for LaInO_3 . To measure the γ angle of LaInO_3 , we perform peak finding of only equivalent oxygen atoms, corresponding to the distance of 2 pseudocubic unit cells (see Fig. 4 (c)), and then we measure the average γ angle across the interface as marked in Fig. 4 (b). The result of our analysis is shown in Fig. 4 (d). We find an γ angle of $88.9^\circ \pm 1^\circ$ in the a_{pc} -oriented LaInO_3 , which is closer to 90° than to the expected equilibrium value of LaInO_3 of 87.6° . As a reference for our measurement, we use the 90° angle in the cubic BaSnO_3 pseudosubstrate.

C. In-Situ Heating Experiment

To examine if LaInO_3 undergoes the phase transitions between the temperature at which the film is grown and room temperature, and to check if differently oriented domains are formed immediately after the LaInO_3 film growth starts or during cooling the film down, we perform an in-situ heating experiment in the temperature range required for the growth of our heterostructures.

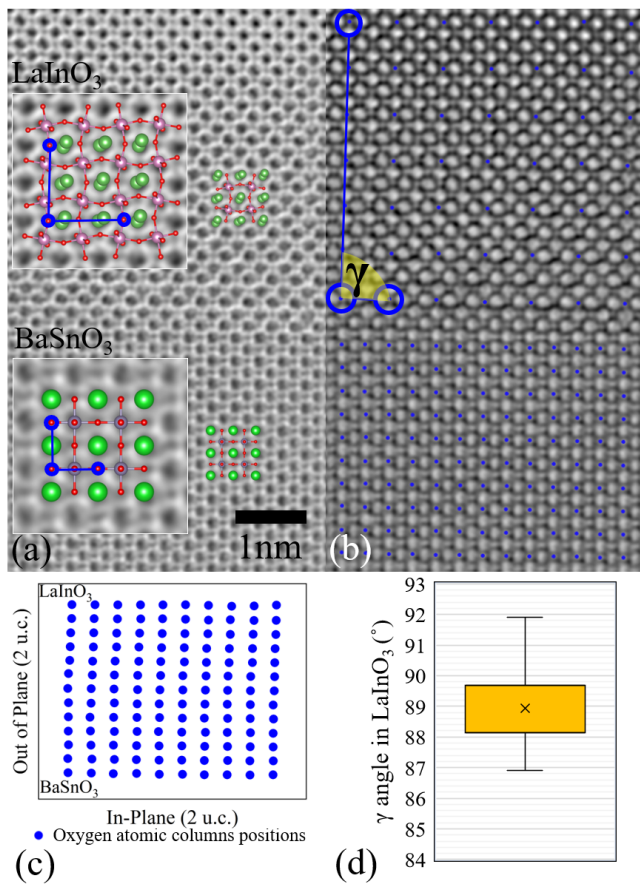


FIG. 4. (a) Amplitude of the exit wave obtained from the exit wave reconstruction of the BaSnO₃/LaInO₃ interface with insets showing the atomic structures of BaSnO₃ and LaInO₃. Dark dots correspond to atoms. (b) Inversed contrast of the amplitude, used for oxygen atomic columns mapping. Oxygen positions used for γ angle measurement are marked with blue dots, and extracted in (c). (d) Graphic representation of the γ angle value in LaInO₃.

Results are shown in Fig. 5. Due to the thermal bending of the heating membrane, it was not possible to record HRTEM images at a fixed sample position. When analyzing the HRTEM images (Figs. 5 (a) and (b)), features like horizontal and vertical stripes, that are specific for orthorhombic domains, can be recognized. Fast Fourier transformed images in Figs. 5 (a) and (b) show that all specific reflexes for LaInO₃ are present, and that the domains stay unchanged up to 650 °C. At 700 °C, due to the lack of the oxygen in the in-situ experiment (which was performed in vacuum), the LaInO₃ film decomposes, and formation of holes starts. The holes in the LaInO₃ film are indicated by white arrows in Fig. 5 (c). Furthermore, the diffraction pattern of the LaInO₃ film at 750 °C is shown in Fig. 5 (d). Diffraction reflexes marked with red, green, and blue are specific only for a_{pc}/b_{pc} , a_{pc}/b_{pc} orientation that is rotated by 90° in the in-plane direction, and c_{pc} orientation, respectively. Presence of all three types of reflexes suggests that these domains stay

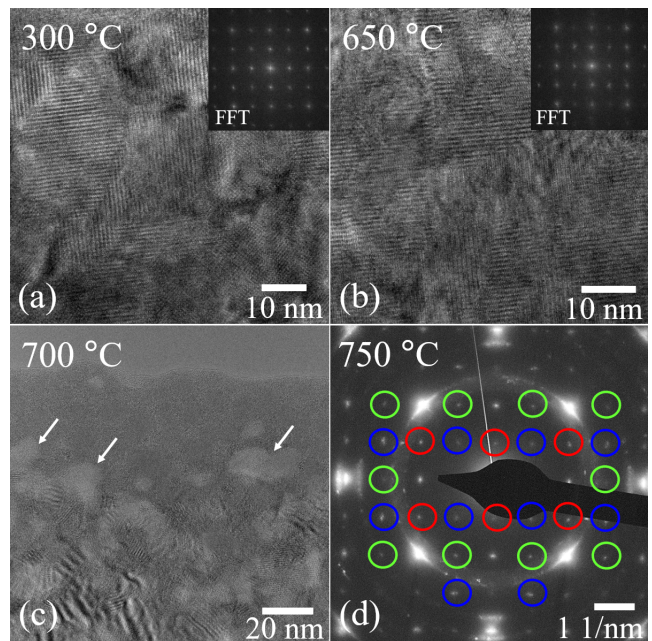


FIG. 5. HRTEM images of the LaInO₃ film heated at (a) 300 °C, (b) 650 °C, and (c) 700 °C (white arrows are pointing at the LaInO₃ film decomposition). Corresponding fast Fourier transformed images (FFT) are overlaid in (a) and (b). (d) Diffraction pattern of the LaInO₃ film at 750 °C, where red, green, and blue correspond to reflexes specific only for a_{pc}/b_{pc} , a_{pc}/b_{pc} orientation that is 90° rotated in the in-plane direction, and c_{pc} orientation, respectively.

stable up to 750 °C. With a more detailed inspection, the elongation of the brightest reflexes that appear for all three orientations can be observed. The elongation appears due to the twisting of domains for a few degrees in the in-plane direction. The fact that reflexes specific for the three differently oriented orthorhombic domains stay stable at the growth temperature indicates that these LaInO₃ domains are most likely formed through epitaxial growth and not by phase transformation during the cool-down.

From our experimental study of coherently grown orthorhombic LaInO₃ on cubic BaSnO₃ we find the main results:

- The epitaxial layer is formed of domains that exhibit three different LaInO₃ epitaxial relationships with respect to BaSnO₃, i.e. c_{pc} and a_{pc}/b_{pc} of LaInO₃ parallel to the BaSnO₃ (100) surface.
- c_{pc} -oriented domains and a_{pc}/b_{pc} -oriented domains appear with similar probability.
- The γ angle of coherently strained a_{pc}/b_{pc} -oriented LaInO₃ on the (001) surface of cubic BaSnO₃ is close to 90°, and deviates from the equilibrium value of 87.6°.
- LaInO₃ domains in the LaInO₃ film are formed from the beginning of the growth process.

V. COMPUTATIONAL RESULTS AND DISCUSSION

A common approach to predict the most favorable orientation relationship in epitaxial growth in heteroepitaxy is to calculate the strain energy density for different orientations considering coherent growth. The orientation with the lowest strain energy is considered as the most favorable one. Using Hooke's law $\sigma_{ij} = C_{ijkl} \cdot \varepsilon_{kl}$, the strain energy density is given by:

$$W = \frac{1}{2} C_{ijkl} \cdot \varepsilon_{ij} \cdot \varepsilon_{kl}, \quad (2)$$

where C_{ijkl} is the stiffness tensor that can be represented in Voigt notation as a 6×6 matrix with 36 independent components, and ε_{ij} represents the strain tensor. In our calculations, we consider a plane stress condition for the thin coherent LaInO_3 film. This means that the stress is induced by the lattice mismatch, and present along the two perpendicular in-plane axes of the film (x- and y-axis), while elastic relaxation along the surface normal (z-direction) requires the components of the stress tensor perpendicular to the growth surface to be zero: $\sigma_{zz} = \sigma_{xz} = \sigma_{yz} = 0$. The axial strain along the two in-plane axes ε_{xx} and ε_{yy} , as well as shearing within the interfacial plane between the x- and y-axis, ε_{xy} , are known. The in-plane strain $\varepsilon_{xx/y}$ in the LaInO_3 layer is equal to the lattice misfit f to the BaSnO_3 pseudosubstrate and is given by the equation:

$$f = \frac{a_s}{a_{l,x/y}} - 1, f = \varepsilon_{xx/yy}. \quad (3)$$

Here, a_s is the lattice constant of the pseudosubstrate (BaSnO_3), and $a_{l,x/y}$ is the lattice constant of the LaInO_3 layer along the x- or y-axis. The unknown parameters ε_{zz} , ε_{xz} , and ε_{yz} are calculated using Hooke's law and the boundary conditions of the stress-free surface. The elastic constants used in the LaInO_3 stiffness tensor are calculated by DFT and shown in Table II.

We distinguish two possible orientations: (i) growth of the c_{pc} -oriented domain where $(001)_{pc}$ is parallel to the (001) surface of BaSnO_3 , and (ii) Growth of the a_{pc}/b_{pc} -oriented domains where $(100)_{pc}/(010)_{pc}$ is parallel to the BaSnO_3 (001) surface. We start with case (i). For this case we can perform the calculation in the orthorhombic coordinate system of LaInO_3 with $[100]_{ortho}/[010]_{ortho}/[001]_{ortho}$ being the x-/y-/z-axis, respectively. The coherency between the epitaxial LaInO_3 film and the cubic BaSnO_3 pseudosubstrate requires that $a_{pc} = b_{pc} = a_{\text{BaSnO}_3}$ and that the angle γ between a_{pc} and b_{pc} becomes 90° . This is obtained if the two orthorhombic in-plane axes are strained such that $[100]_{ortho} = [010]_{ortho} = \sqrt{2} \cdot a_{\text{BaSnO}_3}$. No in-plane shearing between the x- and y-axis is required, i.e. $\varepsilon_{xy} = 0$.

In case (ii), to calculate the strain energy density of a_{pc} - and b_{pc} -oriented films, where $(100)_{pc}$ and $(010)_{pc}$

TABLE III. Summarized strain values (ε) for c_{pc} , a_{pc} and b_{pc} LaInO_3 orientations parallel to the BaSnO_3 (001) surface.

LaInO_3	ε_{xx}	ε_{yy}	ε_{zz}	ε_{yz}	ε_{zx}	ε_{xy}
c_{pc}	-0.019	0.022	-	0	0	0
a_{pc}	$8.9 \cdot 10^{-4}$	$3.4 \cdot 10^{-3}$	-0.002	$1.6 \cdot 10^{-4}$	0	0
b_{pc}	$8.9 \cdot 10^{-4}$	$3.4 \cdot 10^{-3}$	-0.002	$-1.6 \cdot 10^{-4}$	0	0

TABLE IV. Calculated strain energy density for all three growing directions.

Orientation parallel to the (001) BaSnO_3 surface	a_{pc}	b_{pc}	c_{pc}
Strain energy density (GPa)	0.0011	0.0011	0.0480

are parallel to the BaSnO_3 (001) surface, we have to rotate the coordinate system from the orthorhombic system to the pseudocubic so that the x-axis equals either b_{pc} or a_{pc} , respectively, and c_{pc} ($= c_{ortho}$) is the y-axis. Note that for case (ii) the surface normal, the z-axis, does not exactly coincide with the third pseudocubic axis a_{pc} or b_{pc} because the angle between a_{pc} and b_{pc} , γ , equals 87.6° (Fig. 1 (f)). The orthorhombic coordinate system is right hand rotated by $+43.81^\circ$ and -46.17° around the c_{pc} axis in order to obtain a_{pc} - and b_{pc} -oriented films, respectively. The stiffness tensor for the rotated coordinate system is obtained by solving the transformation equation for a 4th rank tensor. Summarized strain values (ε) for all cases are shown in Table III. Results of the strain energy density for each of the three pseudocubic growth directions are presented in Table IV.

Considering that the area occupancy of the differently oriented domains scales with the strain energy density, we found an obvious discrepancy to the data obtained from our TEM analysis. While the calculated strain energy density of a_{pc}/b_{pc} domains (shown in Tab. IV) is by an order of magnitude lower than the one of the c_{pc} domains, both orientations occur with similar probability in the TEM analysis. To address this question, we compute the formation energy of bulk and strained orthorhombic LaInO_3 for different orientations using DFT. We focus on the influence of the experimentally observed deviation of the angle γ from the bulk value in the a_{pc} - and b_{pc} -oriented layers. Since a_{pc} - and b_{pc} -oriented LaInO_3 are symmetry equivalent, we restrict ourselves to a_{pc} - and c_{pc} -oriented LaInO_3 . The formation energy is calculated for a unit cell of LaInO_3 with periodic boundary conditions. For a_{pc} -oriented LaInO_3 , the primitive unit cell is formed by $2 \times 2 \times 2$ pseudocubic unit cells (see Fig. 1 (f)). For the c_{pc} -oriented LaInO_3 , the primitive cell is shown in Fig. 1 (a). The in-plane parameters are fixed to the value of the BaSnO_3 pseudosubstrate, while the atomic positions and the out-of-plane parameters are relaxed. This means that the calculation mimics rather a thick film, but still a coherently strained one. For the a_{pc} orientation along the growth direction, we calculate two distinct cases with (i) γ fixed to 87.6° like in the bulk crystal, and with (ii) γ fixed to 90° , which is closer to the

TABLE V. Formation energies (E_f) per formula unit (f.u.) of a_{pc} - and c_{pc} -oriented LaInO_3 .

LaInO_3	Lattice parameters (Å)			E_f (eV/f.u.)
	a	b	c	
a_{pc} out-of-plane ($\gamma = 87.6^\circ$)	8.23	8.23	8.20	-12.86
a_{pc} out-of-plane ($\gamma = 90^\circ$)	8.23	8.23	8.20	-12.84
c_{pc} out-of-plane	5.82	5.82	8.20	-12.84

experimentally observed angle γ in our epitaxial layers. The formation energy, E_f , is computed as:

$$E_f = E_{tot}^{\text{LaInO}_3} - \sum_{\text{elements}} E_{tot}^{\text{bulk}}, \quad (4)$$

where $E_{tot}^{\text{LaInO}_3}$ and E_{tot}^{bulk} are the total energies of orthorhombic LaInO_3 in the crystalline state and of its constituent elements (La, In, O) in their reference states, respectively.

Table V summarizes the formation energies per formula unit of bulk LaInO_3 for the three different cases, i.e. LaInO_3 coherently strained to BaSnO_3 (001) with c_{pc} and a_{pc} orientation. The LaInO_3 film with a_{pc} along the growth direction, with $\gamma = 87.6^\circ$ (as in the bulk crystal), has the lowest formation energy indicating that it would be the most favorable structure. This result is, as expected, in agreement with that from continuum elasticity theory (see Table IV), where the orientation along a_{pc} is more favorable than the orientation along c_{pc} . Although the difference in formation energy between a_{pc} ($\gamma = 87.6^\circ$) and c_{pc} is only 0.02 eV/f.u., corresponding to 0.0461 GPa, that matches very well the calculated strain energy density value of 0.0480 GPa for the c_{pc} -oriented domain. For a_{pc} -oriented LaInO_3 with $\gamma = 90^\circ$, however, the formation energy is similar to the formation energy of c_{pc} -oriented LaInO_3 . This finding is consistent with the experimentally observed distribution of a_{pc} - and c_{pc} -oriented domains.

In the following, we will address the influence of the BaSnO_3 pseudosubstrate and the $\text{LaInO}_3/\text{BaSnO}_3$ interface, focusing on their effect on the angle γ in the coherently strained LaInO_3 film. We compare formation energies per atom in a heterostructure where LaInO_3 is coherently strained on BaSnO_3 . In our calculation, a supercell consisting of a very thin film of 4 pseudocubic unit cells of LaInO_3 on top of a BaSnO_3 pseudosubstrate is considered. This calculation explicitly includes the interface and its effect on the domain formation. In the case shown in Fig. 6 (a) the a_{pc} orientation of the LaInO_3 film is parallel to the BaSnO_3 (001) surface and γ is fixed to 87.6° . Fig. 6 (b) represents the case where LaInO_3 is relaxed. For comparison, Fig. 6 (c) shows a c_{pc} -oriented film where LaInO_3 is relaxed. A striking observation here is that upon relaxation, the angle γ changes from the equilibrium value of 87.6° to 88.5° . This behavior is in excellent agreement with our TEM measurements.

Table VI summarizes the formation energies per atom for all three cases shown in Fig. 6. Comparing the formation energy of a_{pc} with two different values of γ , we

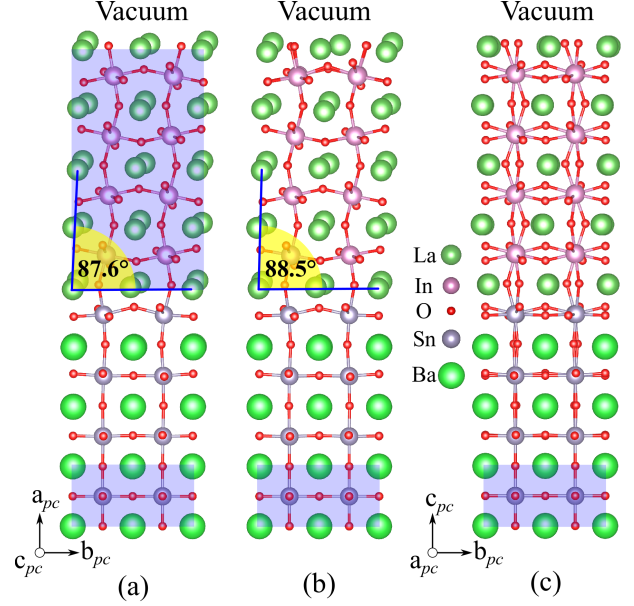


FIG. 6. Geometries of coherently strained a_{pc} ((a) and (b)), and c_{pc} (c) orientation of LaInO_3 on top of BaSnO_3 (001) surface. (a) In LaInO_3 , the blue shadowed region marks the fixed geometry. Blue shadowed regions in BaSnO_3 mark the first unit cell which has lattice parameter fixed to the bulk value.

TABLE VI. Summarized formation energies in eV/atom for coherent growth of LaInO_3 on the BaSnO_3 (001) surface.

LaInO_3	a_{pc} ($\gamma = 87.6^\circ$)	a_{pc} ($\gamma = 88.5^\circ$)	c_{pc}
E_f	-2.419	-2.429	-2.428

find a behavior opposite to that of the bulk LaInO_3 formation energies reported in Table V. The a_{pc} orientation with γ angle as in the bulk is now energetically less favorable than the a_{pc} orientation where γ angle is closer to 90° . The increase of the γ angle (Fig. 6 (b)) decreases the formation energy for the a_{pc} orientation, and shifts it towards that of the c_{pc} orientation. Therefore, the formation energies of relaxed a_{pc} (γ closer to 90°) and c_{pc} orientation become similar, which is in excellent agreement with the domain distribution observed by TEM. This confirms that here the interface is decisive in controlling the epitaxial relationship, instead of the exclusive consideration of continuum mechanics, i.e. strain energy.

To get insight into the role of the interface, we have a closer look on the octahedra tilt pattern of the a_{pc} -oriented interface, and compare it to that of bulk LaInO_3 and bulk BaSnO_3 . As shown in Fig. 7, in bulk LaInO_3 , an alternation of In-O bond lengths within the inequivalent octahedra along the c_{pc} direction can be observed (a_{pc} in the out of plane direction). In contrast, there is no such alternation of the Sn-O bond length in the cubic perovskite BaSnO_3 . Moreover, these bonds are shorter and therefore stronger than the In-O bonds in LaInO_3 .

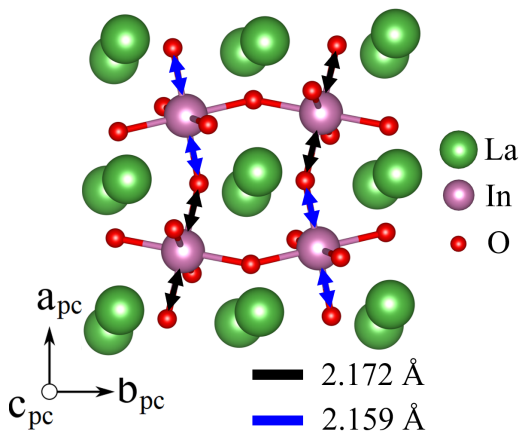


FIG. 7. Alternation of In-O bond lengths in bulk LaInO_3 .

Once a_{pc} -oriented LaInO_3 grows on top of BaSnO_3 (001), the stronger Sn-O bonds force the In-O bonds within the inequivalent octahedra to become equal in length at the interface. In addition, the in-plane La shift is reduced due to the lack of oxygen octahedral tilt in the BaSnO_3 substrate. Therefore, it is the local chemistry of bonding at the interface, i.e. the change in In-O bond length and the shift of the La atoms at the interface due to the BaSnO_3 pseudosubstrate, that leads to an increase of the angle γ to almost 90° . This increase shifts the formation energy in the a_{pc} -oriented LaInO_3 domains. Such balancing of formation energies has a strong impact on the distribution of domains in epitaxial films, i.e both, a_{pc} and c_{pc} , orientations are equally distributed, although from strain energy arguments we would expect a strong preference for the a_{pc} orientation.

VI. SUMMARY AND CONCLUSIONS

In this work, we have presented a combined experimental and theoretical study of the domain structure in orthorhombic LaInO_3 thin films coherently grown on a cubic BaSnO_3 pseudosubstrate. We have shown that the epitaxial layer is formed of domains that correspond to the three different pseudocubic orientations of LaInO_3 . In contrast to a common approach that predicts the preferred orientation relationship between film and substrate based on strain energy density calculations, we have shown that the interface chemistry of bonding may balance the energetics of the system and counteract the strain accommodation. Our finding highlights the remarkable influence of the interface chemistry on the epitaxial relationship in heterostructures of different ABO₃ perovskites with different symmetries.

VII. ACKNOWLEDGEMENTS

This work was supported by the Leibniz Senatsausschuss Wettbewerb (SAW) project BaStet (No. K74/2017) and was performed in the framework of GraFOx, a Leibniz science campus partially funded by the Leibniz Association. We thank the European Community (Europaeischer Fonds fr regionale Entwicklung-EFRE) under Grant No. 1.8/15 for partially funding this project. W. A. acknowledges the North-German Supercomputing Alliance (HLRN) for providing HPC resources that have contributed to the research results reported in this paper - project bep00078. We thank Tore Niermann, Technical University Berlin, for partial support in TEM work. Useful discussion with Tobias Schulz is gratefully acknowledged.

VIII. REFERENCES

- [1] A. Ohtomo and H. Hwang, A high-mobility electron gas at the $\text{LaAlO}_3/\text{SrTiO}_3$ heterointerface, *Nature* **427**, 423 (2004).
- [2] N.-C. Yeh, R. Vasquez, C. Fu, A. Samoilov, Y. Li, and K. Vakili, Nonequilibrium superconductivity under spin-polarized quasiparticle currents in perovskite ferromagnet-insulator-superconductor heterostructures, *Physical Review B* **60**, 10522 (1999).
- [3] L. Bjaalie, B. Himmetoglu, L. Weston, A. Janotti, and C. Van de Walle, Oxide interfaces for novel electronic applications, *New Journal of Physics* **16**, 025005 (2014).
- [4] J. M. Rondinelli and N. A. Spaldin, Structure and properties of functional oxide thin films: insights from electronic-structure calculations, *Advanced materials* **23**, 3363 (2011).
- [5] U. Kim, C. Park, Y. M. Kim, J. Shin, and K. Char, Conducting interface states at $\text{LaInO}_3/\text{BaSnO}_3$ polar interface controlled by fermi level, *APL Materials* **4**, 071102 (2016).
- [6] Y. Kim, Y. M. Kim, J. Shin, and K. Char, $\text{LaInO}_3/\text{BaSnO}_3$ polar interface on MgO substrates, *APL Materials* **6**, 096104 (2018).
- [7] Y. M. Kim, T. Markurt, Y. Kim, M. Zupancic, J. Shin, M. Albrecht, and K. Char, Interface polarization model for a 2-dimensional electron gas at the $\text{BaSnO}_3/\text{LaInO}_3$ interface, *Scientific reports* **9**, 1 (2019).
- [8] H. J. Kim, U. Kim, T. H. Kim, J. Kim, H. M. Kim, B.-G. Jeon, W.-J. Lee, H. S. Mun, K. T. Hong, J. Yu, *et al.*, Physical properties of transparent perovskite oxides (Ba,La)SnO₃ with high electrical mobility at room temperature, *Physical Review B* **86**, 165205 (2012).
- [9] H. J. Kim, U. Kim, H. M. Kim, T. H. Kim, H. S. Mun, B.-G. Jeon, K. T. Hong, W.-J. Lee, C. Ju, K. H. Kim, *et al.*, High mobility in a stable transparent perovskite oxide, *Applied Physics Express* **5**, 061102 (2012).
- [10] H. Inaba, H. Hayashi, and M. Suzuki, Structural phase transition of perovskite oxides LaMO_3 and $\text{La}_{0.9}\text{Sr}_{0.1}\text{MO}_3$ with different size of B-site ions, *Solid State Ionics* **144**, 99 (2001).
- [11] K. J. Choi, S. H. Baek, H. W. Jang, L. J. Belenky, M. Lyubchenko, and C.-B. Eom, Phase-transition tem-

- peratures of strained single-crystal SrRuO₃ thin films, *Advanced Materials* **22**, 759 (2010).
- [12] D. G. Schlom, L.-Q. Chen, C.-B. Eom, K. M. Rabe, S. K. Streiffer, and J.-M. Triscone, Strain tuning of ferroelectric thin films, *Annu. Rev. Mater. Res.* **37**, 589 (2007).
- [13] J. Jiang, W. Tian, X. Pan, Q. Gan, and C. Eom, Domain structure of epitaxial SrRuO₃ thin films on miscut (001) SrTiO₃ substrates, *Applied physics letters* **72**, 2963 (1998).
- [14] D. Proffit, H. Jang, S. Lee, C. Nelson, X. Pan, M. Rzechowski, and C. Eom, Influence of symmetry mismatch on heteroepitaxial growth of perovskite thin films, *Applied Physics Letters* **93**, 111912 (2008).
- [15] J. P. Perdew, A. Ruzsinszky, G. I. Csonka, O. A. Vydrov, G. E. Scuseria, L. A. Constantin, X. Zhou, and K. Burke, Restoring the density-gradient expansion for exchange in solids and surfaces, *Physical review letters* **100**, 136406 (2008).
- [16] V. Blum, R. Gehrke, F. Hanke, P. Havu, V. Havu, X. Ren, K. Reuter, and M. Scheffler, Ab initio molecular simulations with numeric atom-centered orbitals, *Computer Physics Communications* **180**, 2175 (2009).
- [17] R. Golesorkhtabar, P. Pavone, J. Spitaler, P. Puschnig, and C. Draxl, Elastic: A tool for calculating second-order elastic constants from first principles, *Computer Physics Communications* **184**, 1861 (2013).
- [18] K. Momma and F. Izumi, Vesta 3 for three-dimensional visualization of crystal, volumetric and morphology data, *Journal of applied crystallography* **44**, 1272 (2011).
- [19] T. Maekawa, K. Kurosaki, and S. Yamanaka, Thermal and mechanical properties of polycrystalline BaSnO₃, *Journal of alloys and compounds* **416**, 214 (2006).
- [20] H. M. Park, H. J. Lee, S. H. Park, and H. I. Yoo, Lanthanum indium oxide from x-ray powder diffraction, *Acta Crystallographica Section C: Crystal Structure Communications* **59**, i131 (2003).
- [21] A. Glazer, The classification of tilted octahedra in perovskites, *Acta Crystallographica Section B: Structural Crystallography and Crystal Chemistry* **28**, 3384 (1972).
- [22] A. Smith and A. Welch, Some mixed metal oxides of perovskite structure, *Acta Crystallographica* **13**, 653 (1960).
- [23] H. Mizoguchi, H. W. Eng, and P. M. Woodward, Probing the electronic structures of ternary perovskite and pyrochlore oxides containing Sn⁴⁺ or Sb⁵⁺, *Inorganic chemistry* **43**, 1667 (2004).
- [24] A. Bouhemadou and K. Haddadi, Structural, elastic, electronic and thermal properties of the cubic perovskite-type BaSnO₃, *Solid state sciences* **12**, 630 (2010).
- [25] A. Erkişi, G. Gökoğlu, G. Sürücü, R. Ellialtıoğlu, and E. K. Yıldırım, First-principles investigation of LaGaO₃ and LaInO₃ lanthanum perovskite oxides, *Philosophical Magazine* **96**, 2040 (2016).